

## Effect of properties of NC-TiO<sub>2</sub> grains on the performance of organic/inorganic solar cells

H. Al-Dmour <sup>\*a</sup>, D.M. Taylor <sup>b</sup>

<sup>a</sup> *Department of Physics, Faculty of Science, Mutah University, Mutah, 61710, Jordan*

<sup>b</sup> *School of Electronic Engineering, Bangor University, Dean Street, Bangor, LL57 1UT, Gwynedd, United Kingdom*

This work studies the influence of the properties of nanocrystalline -titanium dioxide (nc-TiO<sub>2</sub>) films on the performance of solar cells based on the Organic materials/ncTiO<sub>2</sub> multilayer structure. That was investigated using X-ray diffraction, Atomic force microscopy (AFM), and Source-Measure Unit(SMU) under different ambient conditions. The device produced from batch A exhibit better performance compared to the device produced from batch B. The short circuit current,  $J_{sc}$ , increases from 0.03 mA/cm<sup>2</sup> to 0.22 mA/cm<sup>2</sup>, and the power conversion efficiency,  $\eta$ , from 0.01% to 0.09% in comparison between batches A and B solar cells. That is attributed to the grains of batch A nc-TiO<sub>2</sub> having a size of 25 nm and a height of 100 nm, while particles of batch B nc-TiO<sub>2</sub> film have a height of 40 nm and a size of 19 nm. These features cause to increase in the resistance and defects throughout the bulk region and interfaces of Batch B solar cells and impact the mechanism processes of charge generation of solar cells.

(Received July 24, 2023; Accepted October 6, 2023)

*Keywords:* Grain size, Solar cells , XRD pattern, Rectification ratio, Scherer equation

### 1. Introduction

Solar cell scientists have investigated different materials and various techniques to fabricate solar cells with high efficiency and low costs [1] Organic semiconductors are examples of materials for fabricating solar cells whose properties have the potential to compete with silicon at a much-reduced cost [2]. Organic solar cells are characterized by high optical absorption coefficient (usually  $\geq 10^5$  cm<sup>-1</sup>), low cost of the basic material, the formation of a large interface area, compatible with a flexible substrate, and a good response to high temperature and low light intensities [3]. To enhance their performances, metal oxide materials have been used to fabricate bi-layer solar cells with organic materials [4,5]. These materials are well-known as electron acceptor and transparent layer for applications in solar cells. For example, Shao-Sian Li reported that the efficiency of poly(3-hexylthiophene) (P3HT)/titanium dioxide (TiO<sub>2</sub>) nanorods hybrid bulk heterojunction (BHJ) and nanostructured zinc oxide (ZnO)/P3HT hybrid solar cell is largely dependent on nano morphology of polymer/nanocrystal hybrid [6] . In addition, the mechanism of charge separation and suppressed interface recombination rate in the polymer/inorganic hybrids are affected by the modification of interfacial layers between the hole and electron transport materials [7,8]. That is considered to be an advantage of using nanoparticle metal oxide in solar cells because their structure properties (pore sizes, particles shape, thickness) can be utilized to improve the parameters of solar cells [9].

In this article, we report our study of the fabrication, characteristics, and structural properties of nc-TiO<sub>2</sub> layers produced using two different sol gels of titanium oxide for solar cells application. The results showed that the electrical properties of Polymer /nc-TiO<sub>2</sub> solar cells are affected by the structure of nc-TiO<sub>2</sub> films.

\* Corresponding author: hmoud79@mutah.edu.jo  
<https://doi.org/10.15251/JOR.2023.195.587>

## 2. Experimental method

The Double Layer P3HT/nc-TiO<sub>2</sub> Solar Cells (DLSCs) were fabricated using an organic semiconductor instead of the electrolyte and the dye in DSSC [4]. Two different batches of TiO<sub>2</sub> sol-gel (Ti-Nanoxide T) were purchased from Solaronix SA. According to the supplier, these batches differed from each other only in terms of age which influenced on the first batch (labeled batch A) has higher water/ethanol concentration and lower solid residue than the second batch (labeled batch B) in order to distinguish them. Porous nc-TiO<sub>2</sub> films were readily prepared by spreading a TiO<sub>2</sub> sol-gel over on fluorine-doped, tin oxide (SnO<sub>2</sub>:F) electrodes, pre-coated with a thin, dense layer of TiO<sub>2</sub> (Solaronix, Switzerland). The films were left in air for 10 minutes to dry until its milky color disappeared. Then, they were placed on a hot plate for 110 minutes during which time the temperature was increased from ~ 75°C to 450°C. Afterward, the hot plate was turned off and the temperature allowed to fall naturally to ~70°C at which point the substrate was recovered. A solution of the Poly (3-hexylthiophene) (P3HT) was prepared by dissolving 0.03g of P3HT in 2 ml of chloroform (Sigma Aldrich) in a 20ml glass vial yielding a concentration of 1% w/w. To coat a layer of P3HT on the top of then nc-TiO<sub>2</sub> surface, nc-TiO<sub>2</sub> substrates were placed on the vacuum chuck of an Electronic Micro Systems Ltd. Model 4000. A drop of P3HT in chloroform (15 mg/ml) on the top of the nc-TiO<sub>2</sub> film was allowed to suffuse into this layer for several seconds prior to spin coating at 1000 rpm. Finally, the devices were completed by evaporating an array of 3 mm<sup>2</sup>, circular gold electrodes onto the P3HT. The DC electrical measurements on the solar cells both in the dark and under illumination. Measurements were conducted in air and under different light intensities. Current-voltage (I-V) characteristics were measured using a Keithley model 4200 source-measure unit. The crystal structure of nc-TiO<sub>2</sub> film was investigated using a Philips W3830 X-Ray Meter located in the Chemistry Department, Bangor University. The copper target in this instrument emits X-rays of wavelength ~15.4 nm after filtering using a nicked sheet. Crystalline materials are usually composed of microscopic crystalline (grains) separated from each other by grain boundaries. The grain size is calculated from the Scherrer equation [10]:

$$GS = \frac{\kappa\lambda}{\beta \cos \theta} \quad (1)$$

where GS is the grain size and  $\beta$  is the full width at half maximum of the diffraction peak.

Therefore, it becomes possible to investigate the effect of sintering on the nanostructure of the nc-TiO<sub>2</sub> layer. Figure 1 shows the system in which the solar cells were mounted on a copper stage insider vacuum chamber. The vacuum system was composed of a steel chamber connected to a rotary pump and a silicone oil diffusion pump. For electrical measurements, contact was made to the solar cells using fine gold wire and silver paste to connect the electrodes with Keithley instrument.

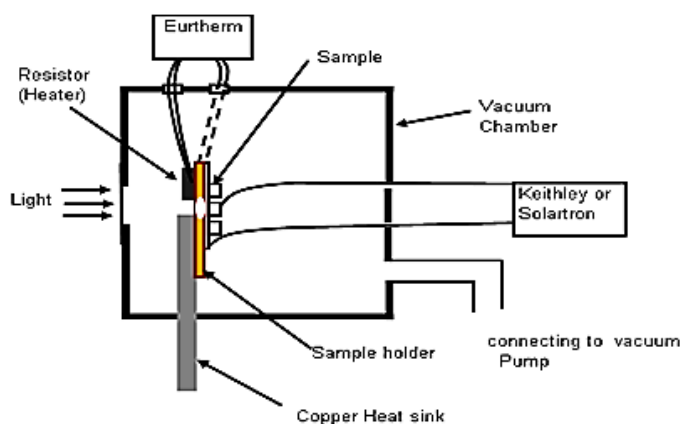


Fig. 1. Schematic representation of the vacuum system and sample holder used in this work.

### 3. Result and Discussion

Figure 2 shows the XRD signal of nc-TiO<sub>2</sub> films produced from batch A. It was observed a strong diffraction peak which occurred at a Bragg angle of 2θ ~ 25°, while smaller peaks were observed near 38°, 48° and 54° and corresponded to reflections from the 101, 004, 200, and 105 lattice planes of the particles. These lattice planes occur in a tetragonal system and correspond to the anatase phase of TiO<sub>2</sub>.

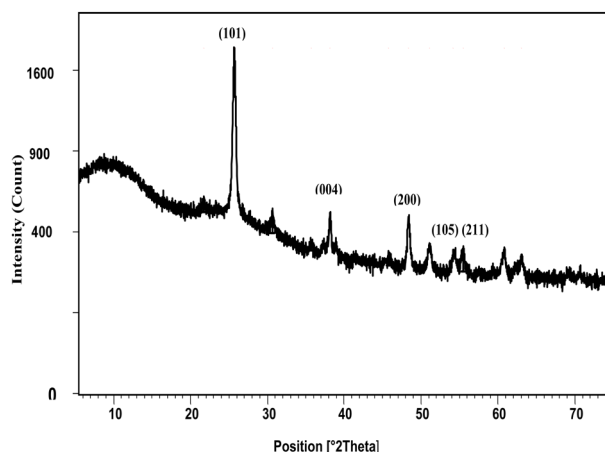


Fig 2. XRD pattern of nc – TiO<sub>2</sub> for batch A.

In Table 1 are given the values of the various parameters describing the difference peaks in Figure 2. These can be used to determine the grain size by applying the Schreer equation (1) to the largest diffraction peak i.e the peak occurring at 2θ=25.6987° for the reflection from the 101-lattice plane. Substituting the following values in Eq. (1):  $\beta = 0.00584$  radians,  $\cos 12.85^\circ = 0.96$ , and  $K = 0.96$ , the grain size is estimated to be 25.6 nm.

Table 1. The parameters of the lattice planes extracted from XRD nc-TiO<sub>2</sub> film from batch A.

Pos. [°2θ.]	Height [cts]	β [°2Th.]	d-spacing [Å]	Rel. Int. [%]	Lattice index
25.6987	1279.44	0.3346	3.47	100	(101)
38.1801	198.41	0.1673	2.36	15.5	(004)
48.3831	221.22	0.3346	1.88	17.3	(200)
54.1584	65.25	0.4684	1.69	5.1	(105)
55.5089	94.76	0.4015	1.66	7.41	(211)

Figure 3 shows the XRD pattern of nc-TiO<sub>2</sub> from batch B. The strongest diffraction peak again appears at 2θ ~ 25.6987°, with weaker peaks appearing near 38°, 48°, and 54°. Again, the presence of these peaks indicates the existence of the anatase phase in the nc-TiO<sub>2</sub> film produced from batch B (similar to nc-TiO<sub>2</sub> produced from batch B).

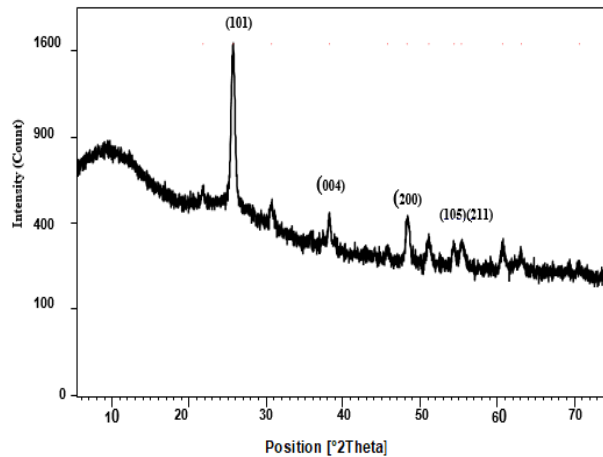


Fig 3. XRD pattern of nc – TiO<sub>2</sub> for batch B.

Table 2 shows the lattice parameters of the nc-TiO<sub>2</sub> film produced from batch B extracted from the XRD spectrum in Figure 3 from which we see a difference regarding the intensity of the peaks and the full width at half maximum ( $\beta$ ) between nc-TiO<sub>2</sub> films produced from batches A and B. By comparing tables 1 and 2, we note that the intensities of the diffraction peaks for nc-TiO<sub>2</sub> from batch A are higher than from batch B. However, the value of  $\beta$  for the nc-TiO<sub>2</sub> from batch B is larger than that from batch A. Therefore, the nc-TiO<sub>2</sub> films produced from batches A and B will have different grain sizes. The lattice parameters from Table 2 for the strongest diffraction peak ( $2\theta = 25.6949^\circ$ ) for the 101 lattice plane are  $K = 0.94$ ,  $\lambda = 0.154$  nm,  $\text{FWHM} = 0.00759$  radians,  $\cos(12.8493) = 0.96$ , yielding a grain size of 19 nm for the nc-TiO<sub>2</sub> film of batch B. Thus the grain size of nc-TiO<sub>2</sub> produced from batch A is bigger than batch B.

Table 1. The parameters of the lattice planes extracted from XRD nc-TiO<sub>2</sub> film from batch B.

Pos. [°2 $\theta$ .]	Height [cts]	$\beta$ [°2Th.]	d-spacing [Å]	Rel. Int. [%]	Lattice index
25.6949	1141.37	0.4349	3.47	100	(101)
38.2623	124.41	0.3346	2.35	10.9	(004)
48.3112	165.11	0.5353	1.88	14.47	(200)
54.398	83.93	0.4015	1.69	7.35	(105)
55.3813	89.52	0.3346	1.66	7.84	(211)

It is known that differences in grain size are important in determining the optical and electronic properties of nc-TiO<sub>2</sub> films (11) and it is expected that the larger grain size should lead to a higher conductivity. Figure 4 shows (J) versus voltage (V) applied for typical DLSC produced from batch A when the voltage was swept from -1 to 1 V. In the dark, the current is lower when the bias was swept from 0 to -1 V compared to the opposite sweep direction. As can be seen from Figure 4, the devices displayed good diode characteristics. The forward current turned on at  $\sim 0.63$  V and by 0.8 V had risen to  $\sim 10$  mA/cm<sup>2</sup>. The reverse current at -0.8 V was  $\sim 0.001$  mA/cm<sup>2</sup>, giving a rectification ratio of  $10^4$ . Under illumination, the rectification ratio decreases to  $10^2$  – and the reverse current increase 0.01 to 1 mA/cm<sup>2</sup> at -0.8 V. This is attributed to the change in conductivity of the bulk region of the components of solar cell. For the region between -1 to 0 V (under the reverse bias condition), the increase in photocurrent occurs because of the addition of free charges carriers when the light is absorbed in the active layers [12]. In contrast, there was a small increase in forward bias current under illumination, from the turn voltage to +1 V related to the small enhancement of majority charge carriers, which was already high in the dark.

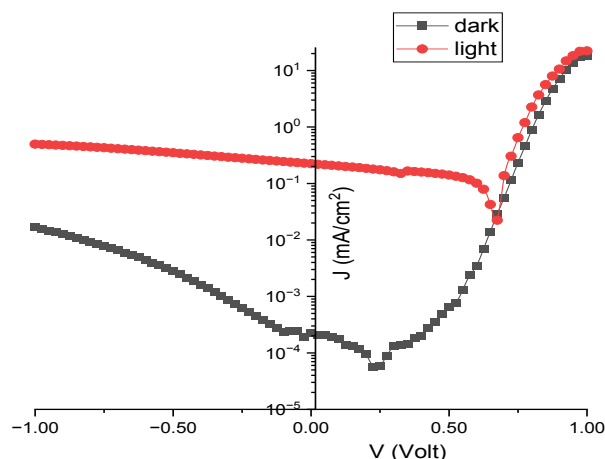


Fig. 4. Log current density–voltage characteristics of the DLSC produced from batch A.

Figure 5 shows the J-V characteristics of the P3HT/nc-TiO<sub>2</sub> solar cell produced from batch A in the linear scale. From Figure. 4, Under illumination with the halogen lamp (100 mW/cm<sup>2</sup>), the device produced an open circuit voltage, Voc, ~0.68 V, short-circuit current density, Jsc ~0.22 mA/cm<sup>2</sup> with fill factor of ~46% yielding a power conversion efficiency of 0.09%. The spread in these values for 10 different cells fabricated on different substrate gave 0.1 < Jsc < 0.22 mA/cm<sup>2</sup> and 0.65 V < Voc < 0.68 V. These results especially for Voc are similar to values reported previously for cells of this type [13], and are believed to arise from the presence of a built-in electric field at the interface between the nc-TiO<sub>2</sub> and the P3HT. Interestingly, Jsc for these devices were similar to generally reported values [14], but are still low compared to dye-sensitized solar cells and polymer/fullerene bulk heterojunction solar cells. Under high forward bias, the present devices exhibit a higher current under illumination in comparison with the dark current at the same condition, around 3 mA/cm<sup>2</sup> at V = 0.8. This suggests that photoconductivity is occurring in the bulk semiconductor region of device.

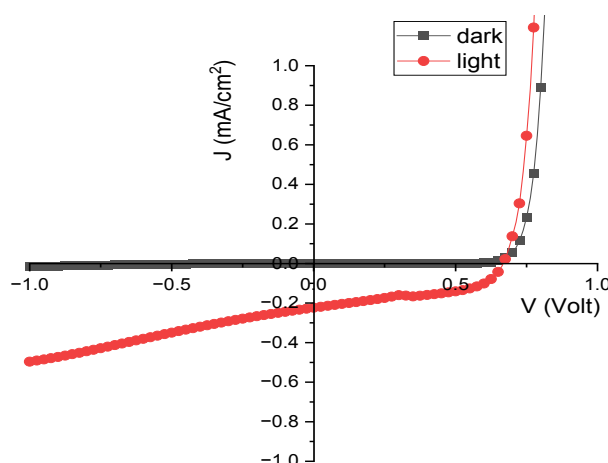


Fig. 5. current density–voltage characteristics of DLSCs produced from batch A.

The J-V characteristics of a DLSC from batch B are shown in linear and semilog form in Figures 6 and 7 respectively. In the dark, the turn-on voltage was 0.75 V with the current rising to ~0.1 mA/cm<sup>2</sup> at 1V and  $4.5 \times 10^{-3}$  mA/cm<sup>2</sup> at -1 V giving a rectification ratio of ~700. While batch B devices demonstrated a higher turn-on voltage, the dark currents were significantly lower in both polarities. Under illumination this device gave a Jsc ~0.03 mA/cm<sup>2</sup>, Voc~0.83 V, and a fill factor of ~ 47% yielding a power conversion efficiency of 0.02% i.e., almost an order magnitude

lower than for the batch A device. The spread in values for 10 devices from different substrates were as follows:  $0.02 \text{ mA/cm}^2 < J_{sc} < 0.04 \text{ mA/cm}^2$  and  $0.78 \text{ V} > V_{oc} > 0.83 \text{ V}$ . At high forward bias, there was little difference between the dark current and that under illumination, suggesting that photoconductivity is very small. This is attributed to the presence of a high resistance in the bulk semiconductor and poor contact between nc-TiO<sub>2</sub> and P3HT.

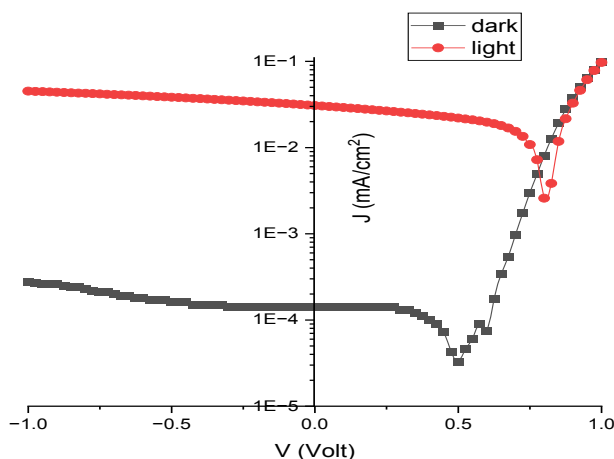


Fig. 6. Log current density–voltage characteristics of the DLSC produced from batch B.

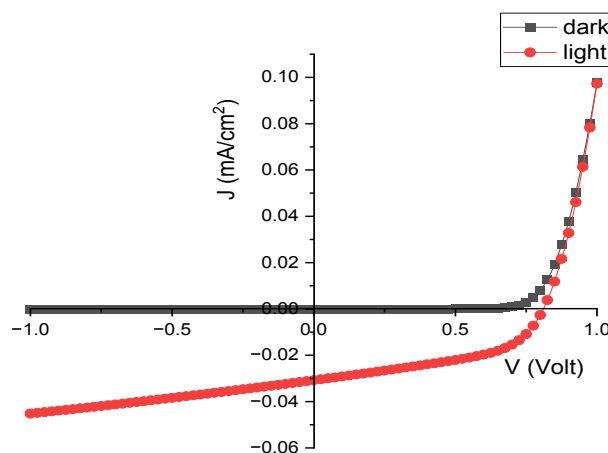


Fig. 7. Current density–voltage characteristics of DLSCs produced from batch B.

Table 3 provides key comparative data obtained from randomly chosen pixels from a number of substrates produced at different times for P3HT/nc-TiO<sub>2</sub> DLSCs produced from batches A and B when illuminated by the halogen lamp ( $72 \text{ mW/cm}^2$ ).

Table 3. Mean and standard deviations of the short circuit current density,  $J_{SC}$ ,  $V_{OC}$ , FF,  $\eta_e$  for the devices produced from batches A and B.

Parameter	Batch A	Batch B
$J_{SC}$ (mA/cm <sup>2</sup> )	0.223±0.006	0.03±0.0006
$V_{OC}$ (V)	0.675±0.02	0.825±0.18
FF (%)	46±3.8	47±4.4
$\eta_e$ (%)	0.09±0.01	0.02 ±0.001

For more details about the properties of nano particles of nc-TiO<sub>2</sub> films, Figures 8-a and 8-b show histogram of particle heights for the batch A nc-TiO<sub>2</sub> films coated with P3HT. Here, the RMS roughness and a mean height of the particles was 10 nm and 40 nm for of batch B nc-TiO<sub>2</sub>/P3HT film while RMS roughness and a mean height of the particles was 18 nm and 103 nm for of batch A nc-TiO<sub>2</sub>/ P3HT film [15].

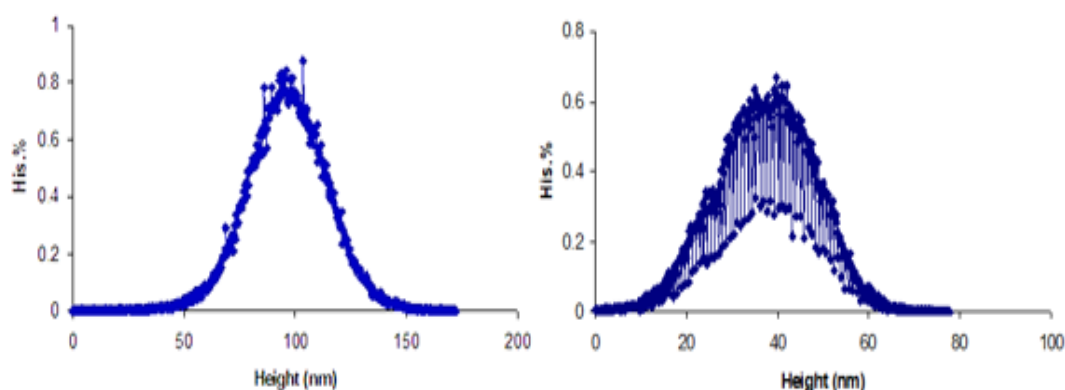


Fig. 8. Distribution of grain height for a nc-TiO<sub>2</sub> film produced from (a) batch A coated with P3HT layer (b) batch B coated with P3HT layer.

More investigation was carried out on the best solar cells here. figure 9 shows the effect of light intensity on the J-V characteristics of the batch A DLSC. The current increases from 0.01 to 0.36 mA/cm<sup>2</sup> at -1V as the light intensity increases, a consequence of increased charge generation. At high forward bias, increasing the light intensity has little effect on the forward current, confirming that photoconduction in the bulk semiconductor is small.

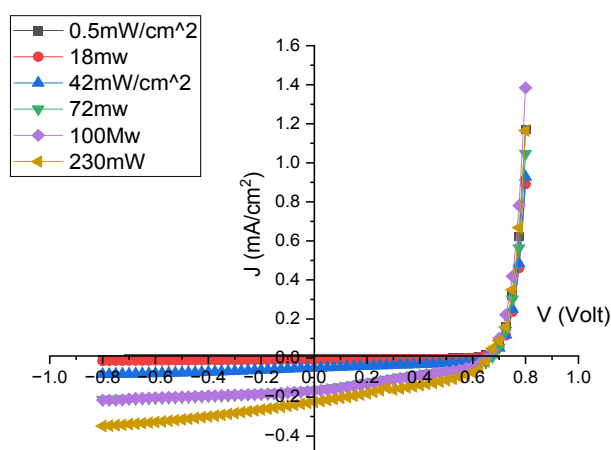


Fig. 9. Effect of the light intensity on the I-V characteristics of Batch A DLSCs.

The effect of light intensity on  $J_{sc}$  is plotted for a batch A device in Figure 10. The relationship between the short circuit current density and the light intensity is reported to be of the form [16].

$$J_{sc} \propto I_{in}^n \tag{2}$$

where  $I_{in}$  is the incident light intensity,  $n$  a factor whose value is determined by the nature of exciton recombination in the device. From the plot in Figure 10, we estimated that  $n \sim 0.88$ .

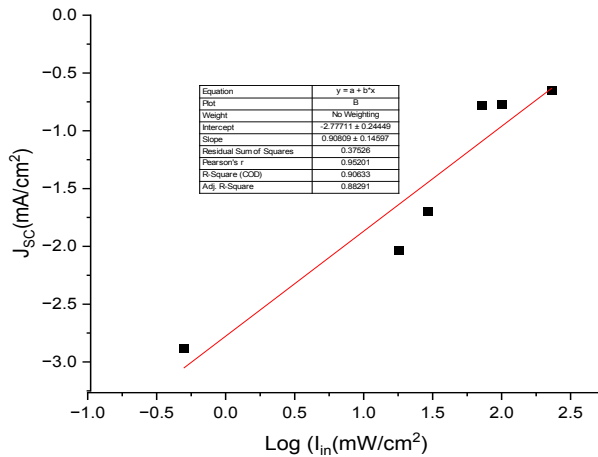


Fig. 10. Dependence of  $J_{sc}$  on incident light intensity for a batch A DLSC.

Figure 11 shows the variation of  $V_{oc}$  with incident light intensity. For low light intensity,  $V_{oc}$  was initially  $\sim 0.5$  V then increased to reach 0.675 V at  $100 \text{ mW/cm}^2$ . However, as the light intensity increased to  $230 \text{ mW/cm}^2$  a slight decrease occurred to 0.65 V.

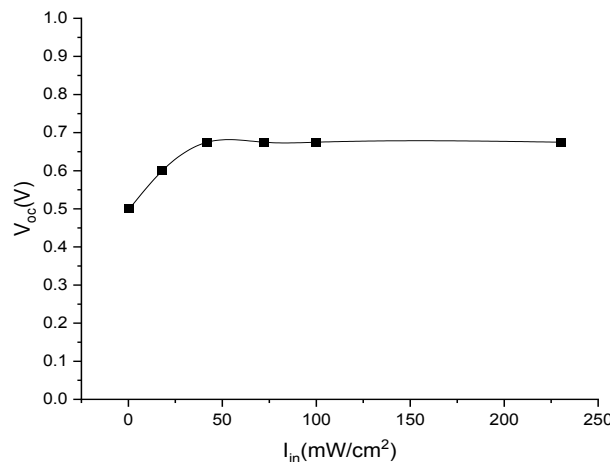


Fig. 11. Dependence of  $V_{oc}$  on incident light intensity for a batch A DLSC.

Under illumination, the device exhibits similar characteristics to a photodiode except with free electrons and holes created by dissociation of excitons in the field of the depletion region. The open circuit voltage will be limited to some maximum value determined by the built in potential  $\sim 0.8$  V, although this may be reduced by the presence of an interfacial dipole layer. In batch A DLSC, Large grains sizes of  $nc\text{-TiO}_2$  film make a good contact between the P3HT and  $nc\text{-TiO}_2$  and

enhanced the number and size of pores on nc-TiO<sub>2</sub> film. That lead to improve the penetration of P3HT through their pores and a significantly increase surface area. Contrary, small grain size and height of nc-TiO<sub>2</sub> film led to reduce the space between the grain and decrease the number of holes. This argument agrees with results published in 2005 [17] by Menda et al. He reported that not only complete interfacial contact, achieved by complete wetting of the TiO<sub>2</sub> surface is essential but also the complete filling of pores is crucial for high efficiency cells. Additionally, it has been reported the negative side effect when the grain radius is comparable to the depletion layer width in tin oxide quantum dot gas sensors [18]. That may explain the increase of efficiency of batch A solar cells in comparison with bath B solar cells. The large size grain in nc-TiO<sub>2</sub> improve the charge separation accurse at interface unlike the batch B solar cells with small grain size.

Light intensity was seen to affect the measured values of Voc and Jsc. The value of Jsc increased with increased light intensity through an increased generation rate. Equation 2 shows also that Jsc increases when the value of Rs decreases. This can occur through increased photoconductivity in the semiconductor by increasing the light intensity. The plot of log Jsc versus light intensity yields an almost linear relation with n equal to 0.88 indicating the presence of a bimolecular recombination process. The Voc of DLSCs increase from 0.45 to 0.7 V when the light intensity increased from 1 mW/cm<sup>2</sup> to 72 mW/cm<sup>2</sup>. This is attributed to an increase in the photo generated current in the devices.

#### 4. Conclusion

We have studied the effect of grains properties of nc-TiO<sub>2</sub> films on the performance on P3HT/nc-TiO<sub>2</sub> solar cells. The result shows differences in J-J characteristics of solar cells produced from two different batches (A, B) under dark and light condition.

The device produced from batch A exhibit better performance compared to the device produced from batch B. The short circuit current, J<sub>sc</sub>, increase from 0.03 mA/cm<sup>2</sup> o 0.22 mA/cm<sup>2</sup>, and the power conversion efficiency, η, from 0.01% to 0.09% in comparison between Batches A and B solar cells. That is attributed to large grain size of batch A nc-TiO<sub>2</sub> film which lead to increase the interfacial area and improve the charge separation

#### Acknowledgments

The authors thank the J A Cambridge (School of Electronic Engineering, Bangor University) for undertaking the IV and XRD measurements, Solaronix Co. for helpful advice on the sintering of the TiO<sub>2</sub> sol-gel.

#### References

- [1] N. Asim, K. Sopian, S. Ahmadi, K. Saeedfar, M.A. Alghoul, O. Saadatian, S.H. Zaidi, *Renewable Sustainable Energy Rev.* **16**, 5834 (2012); <https://doi.org/10.1016/j.rser.2012.06.004>
- [2] P. Troshin, R. Lyubovskaya, and V. Razumov, *Nano technol. Russia*, **3**, 242 (2008). <https://doi.org/10.1134/S1995078008050029>
- [3] J. Chuan, L. Tianze, H. Luan, and Z. Xia, *JPCS*, **276**, 012169 (2010); <https://doi.org/10.1088/1742-6596/276/1/012169>
- [4] B. O'Regan, and M. Gratzel, *Nature*, **353**, 737 (1991); <https://doi.org/10.1038/353737a0>
- [5] H. Al-Dmour, R.H. Alzard, H. Alblooshi, K. Alhosani, S. AlMadhoob, N. Saleh, *Font.Chem.* **561**, 1 (2019); <https://doi.org/10.3389/fchem.2019.00561>
- [6] S. Sian, L. Yun, W. Su, C. Chen, *IEEE J. Sel. Top. Quantum Electron*, **16**, 1635 (2010); <https://doi.org/10.1109/JSTQE.2010.2040948>
- [7] T. Xu, Q. Qiao "Energy Environ. Sci", **4**, 2700 (2011); <https://doi.org/10.1039/C0EE00632G>
- [8] N. Saleh, S. Al-Trawneh, H. Al-Dmour, S. Al-Taweel, *J. Fluoresc.* **25**, 59 (2015); <https://doi.org/10.1007/s10895-014-1479-8>

- [9] S. Bakri, M.Z. Sahdan, F. Adriyanto, et al., AIP Conf. Proc. **1788**, 030030 (2017).  
<https://doi.org/10.1063/1.4968283>
- [10] M. Rabiei, A. Palevicius, A. Monshi, S. Nasiri, A. Vilkauskas, A.G. Janusas, J. Nanomater, **10**, 1627 (2020); <https://doi.org/10.3390/nano10091627>
- [11] D.G. Lee, et al., Appl. Surf. Sci. **7**, 1437 (2017); <https://doi.org/10.1016/j.apsusc.2017.11.124>
- [12] H. Al-Dmour, D.M. Taylor, Appl. Phys. Lett, **94**, 223309 (2009);  
<https://doi.org/10.1063/1.3153122>
- [13] M.Y. Song, K.J. Kim, D.Y. Kim, Sol. Energy Mater. Sol. Cells, **85**, 31 (2005);  
<https://doi.org/10.1016/j.solmat.2003.12.018>
- [14] Watanabe, A. Kasuya, Thin Solid Film, **483**, 358, (2005);  
<https://doi.org/10.1016/j.tsf.2004.12.056>
- [15] H. Al Dmour, East Eur. J. Phys. (4), 171 (2022); <https://doi.org/10.26565/2312-4334-2022-4-17>
- [16] U. Mengesha, T. Yoannes, Solar Energy Materials and Solar Cells, **90**, 3508, (2006);  
<https://doi.org/10.1016/j.solmat.2006.05.010>
- [17] S. Menda, M. Grätzel, Thin Solid Film, **500**, 296 (2006);  
<https://doi.org/10.1016/j.tsf.2005.11.020>
- [18] J. Liu, J. Lv, J. Shi, L. Wu, L. Wu, N. Su, C. Fu, Q. Zhang, J. Mater. Res. Technol, **9**, 16399 (2020); <https://doi.org/10.1016/j.jmrt.2020.11.107>